

## Automatic identification of sites prone to topographic seismic amplification effects by the current seismic codes

P.L. Fantozzi<sup>a,\*</sup>, E. Paolucci<sup>b</sup>, P. Pieruccini<sup>c</sup>, D. Albarello<sup>a,d</sup>

<sup>a</sup> Dipartimento di Scienze Fisiche, della Terra e dell'Ambiente, Università degli Studi di Siena, Siena, Italy

<sup>b</sup> Dipartimento di Fisica e Astronomia, Università di Bologna, Bologna, Italy

<sup>c</sup> Dipartimento di Scienze della Terra, Università degli Studi di Torino, Turin, Italy

<sup>d</sup> Consiglio Nazionale delle Ricerche, Istituto di Geologia Ambientale e Geoingegneria, Rome, Italy

### ARTICLE INFO

#### Keywords:

Topographic seismic amplification effects

Seismic codes

Morphometric analysis

GIS

ArcPy

Python

### ABSTRACT

Current seismic codes provide proxies to estimate seismic amplification effects expected in correspondence of some morphological features. To make possible any empirical validation of these proxies, these features must be univocally identified on the basis of an automatic procedure. To this purpose, based on geomorphological considerations, a GIS-based numerical approach has been developed. The results of a morphometric analysis allowed the correct identification and mapping of the landforms of concern, at a detail corresponding to the resolution of the available digital elevation model (DEM). Some case-studies are provided to show the feasibility of the proposed approach.

### 1. Introduction

Geomorphological settings and the corresponding specific landforms may affect seismic ground motion due to focusing/defocusing of seismic waves, diffraction of body and surface waves and seismic resonance of topographic features (e.g. Refs. [1–3]). Sharp and/or rounded ridges, steep slopes and escarpments, isolated peaks and hilltops are among the most common landforms that may be responsible for amplification effects. These features are considered in two seismic codes adopted in Italy: Working Group on Seismic Microzoning - Gruppo di lavoro MS, 2008 (henceforth SMG08 [4]) and NTC, 2018 (henceforth NTC18 [5]). These two codes have been developed in different contexts. The first one is devoted to the anti-seismic design of single structures in line with more advance international seismic codes. The second has been developed in the frame of seismic microzoning (SM) studies and mainly aims at the characterization of seismic effects at the scale of a municipality for urban planning purposes. The two codes were developed independently and provide different outcomes as a function of the respective targets. The landforms considered in the two codes are very common in geodynamically active regions such as Italy, where recent and ongoing tectonic vertical uplift drives continuous valley downcutting and landscape rejuvenation, leading to high relief energy, slope retreats along watersheds and formation of almost continuous ridges in most drainage

basins. Moreover, the Italian historical urban landscape in hilly and mountain ranges consists typically of small-to medium-sized towns and villages on hilltops or along ridges [6]. Geomorphometry is therefore the main tool (e.g. Refs. [7–13]) for quantitative analysis and interpretation of multiscale landforms from large scale (i.e. the dimensions of a single building) to small scale (i.e. covering large areas or regions). There is extensive literature (see Ref. [14] for a review) on observed amplification/deamplification phenomena affecting seismic ground motion due to geomorphological heterogeneities. However, experimental evaluation of them is hampered by the coexistence of effects induced by the local seismo-stratigraphic settings and by the difficulty of selecting reference sites where these effects can be assumed absent. To tackle this problem, 2D-3D numerical modelling is used [14–17]. Managing these complex numerical tools requires specific skills that generally cannot be expected of engineers and geologists (i.e., practitioners) charged with professional evaluation of local seismic response. Since these methods are computationally expensive, they cannot be applied massively to wide areas, as in SM studies.

To overcome these difficulties, proxies have been proposed to provide a preliminary evaluation of expected topographical effects. These proxies are deduced by extensive parametric analysis of simplified 2D topographic features [18] that approximate and generalize the landform observed in the field. These proxies are also used for regional studies to

\* Corresponding author.

E-mail address: [fantozzi@unisi.it](mailto:fantozzi@unisi.it) (P.L. Fantozzi).

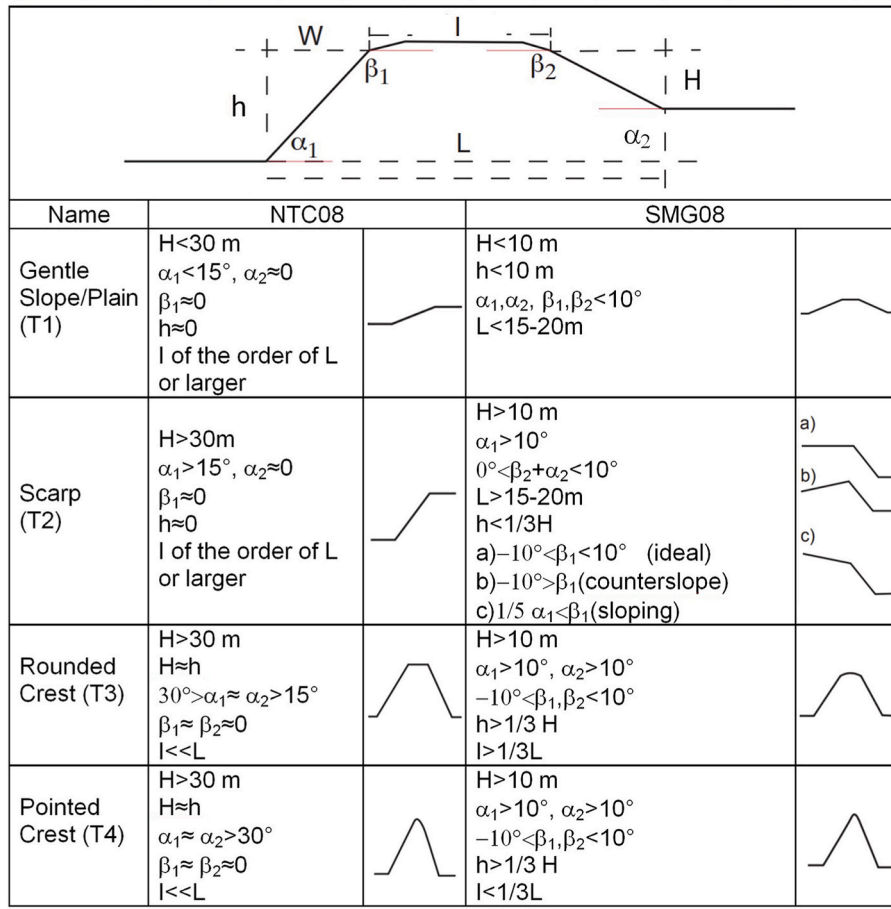


Fig. 1. Standard morphologies prone to ground motion amplification phenomena by the Italian seismic codes NTC18 and SMG08. Note that in NTC18, H and h have the same meaning, and that the depressions of slopes  $\alpha_1$  and  $\alpha_2$  are simply considered to be the average dips of slopes defined as "i". NTC18 codes indicate "crest" as synonymous with ridge or ridgeline.

identify areas potentially prone to topographical effects where more detailed studies are mandatory for a correct evaluation of local seismic response. Some of these proxies have been implemented in the most recent seismic codes (e.g. Refs. [4,5]).

A problem arises in their application since these simplified models should be matched with a wide variety of observed geomorphological features. This requires expert-based analysis which makes the application of these proxies potentially controversial. This difficulty is also enhanced by the fact that to generalize outcomes of numerical analysis, the geometric elements considered are provided in terms of scale-free parameters (direction of slopes and slope angles), which are not sufficient for univocal identification of the morphologies. These drawbacks hamper extensive application of the proxies in the current practice.

The aim of the work is to overcome these difficulties by identifying an automatic analysis workflow that allows the identification of sites possibly subject to seismic topographical amplification effects, which unlike those currently proposed in the bibliography allows to eliminate ambiguity on the choices of the analysis and excessive generalizations of geometric data and morphological maps. The proposed methods are based on numerical procedures based on spatial analysis and finally provide detailed maps and data where such effects are possible (and in some cases documented, as demonstrated for the test area), producing a detailed mapping of the dangerous zone areas in the light of current codes on seismic risk. We will not enter the discussion about the validity of the amplification factors provided in these codes: Anyway, the correct unequivocal identification of these morphologies is a basic prerequisite for the widespread application of any validation procedure of the amplification factors provided by the codes.

In the following, we first summarize code/guideline prescriptions by focusing on major ambiguities, then we state a set of restrictive criteria for the definition of formalized procedures to detect landforms potentially affected by topographic amplification effects. The spatial analysis is performed by GIS platform based on ArcPy™ [19] and Python [20] programming languages, implementing the above criteria. Finally, some case studies illustrate the feasibility of the numerical approach here proposed.

## 2. Morphological proxies based on Italian national codes

Two proxies to assess topographical amplification affects were implemented in the SMG08 [4] and NTC18 [5] codes for engineering design and SM studies, respectively [6], providing different parameterizations of expected effects as outcome. SMG08 considers the adimensional *amplification factors* (Fa) computed for a set of natural resonance periods of structures defined as: (1)

$$\frac{1}{TA_{out}} \int_{0.5TA_{out}}^{1.5TA_{out}} SA_{out}(T) dT \quad (1)$$

$$\frac{1}{TA_{inp}} \int_{0.5TA_{inp}}^{1.5TA_{inp}} SA_{inp}(T) dT$$

where  $SA_{out}(T)$  and  $SA_{inp}(T)$  are the acceleration response spectra of ground motion at the top and at bottom of the relief, respectively;  $TA_{out}$  and  $TA_{inp}$  are the period of their maximum spectral ordinates in the period range 0.1–0.5 s. As concerns NTC18, amplification is provided by another dimensionless parameter (St), which is a multiplier factor for the whole response spectrum. In both cases, the relevant amplification parameters are assessed for standardized landforms characterized by 2D

**Table 1**  
Summary and descriptions of the morphometric parameters of Fig. 1.

Parameter	Description	Dimension	Assumed constraints for spatial analysis
H	Maximum elevation of the slopes	meter	
h	Minimum elevation of the slopes	meter	30 m < h < 160 m,
I	Width of the crest or of the scarp edge	meter	Ridge: I > 300 m Scarp: I < 300 m
W	Width of the slope		W < 600 m both for scarp(I > 300 m) and ridge (I < 300)
L	In the case of crests: overall width of the relief.	meter	80 m < L < 1000 m,
$\alpha_1$ and $\alpha_2$	Dip angle at the bottom of the slopes: the value of $\alpha_1$ and $\alpha_2$ must respect the position of the maximum and minimum difference of elevation ( $\alpha_1 \in H$ and $\alpha_2 \in h$ ).	degree or radiant	
$\beta_1$ and $\beta_2$	Dip angle at the top of the hill for crest	degree or radiant	

topographic profiles ideally traced along the maximum slope of a relief Fig. 1.

These morphometric proxies (Fig. 1 and Table 1) consider ridges (or crests/cliffs), scarps (or escarpments) and slopes to be responsible for seismic amplification effects. Both sets of proxies identify almost symmetrical slopes as the main requirement for ridges, whereas asymmetrical slopes are typical of scarps. Summarizing, SMG08 assumes that:

- only features with  $H > 10$  m and  $\alpha_{1-2} > 10^\circ$  are considered as relevant;
- ridges are defined when  $h \geq H/3$
- scarps are defined when  $h < H/3, \beta_{1-2} < \alpha/5$  and  $I = 15-20$  m or  $I=H$ .

NTC18 proposes a simplified classification identifying ridges where:

- $I < L$  and  $H > 30$  m
- $\alpha_1 = \alpha_2 = \alpha > 15^\circ$

Univocal application of these criteria is hampered by the lack of some key information. In fact, no definition is provided regarding the reference level for determining H and h values (i.e. absolute elevation or difference in elevation? the local base-level?). The implicit assumption is that a relief rises from a wide plain (with slope  $< 10^\circ$  or  $15^\circ$  for SMG08 and NTC18, respectively) whose extension is presumably much larger than L. However, this setting is usually unrealistic in Italy, where the geomorphological setting and related landscape are rugged due to the high relief-energy associated with tectonically active mountain chains and ranges of hills. To side-step this problem and make it possible to apply the criteria of SMG08 and NTC18, further assumptions are therefore necessary. Considering ridges and scarps, we assume that these landforms start from the summit of the relief bordered by two valleys whose bottoms (lowest elevation) coincide with a new ascending slope. The local valley bottom close to the ridge is taken to be the reference level for the elevation h (or H) of the relief (Fig. 1 and Table 1). Nor do SMG08 and NTC18 provide information about the dimensions L, I and W. Some studies have focused on these parameters (e.g. Refs [ 2,15]). suggesting that amplification effects are expected when the overall dimension L is of the order of the seismic wavelength  $\lambda$  of potential interest. To be applied, this suggestion implies the choice of a reference vibration period for ground motion, the seismic phase of interest and the corresponding phase velocity. Since most buildings have resonance periods of about 1 s, we assume that this value identifies the ground vibrations of major interest for engineering purposes. Along the same lines, we assume that shear waves play a major role in the horizontal ground motion responsible for damage. We also assume that topographical effects play a major role (with respect to seismostratigraphic effects) where stiff soils outcrop. With these assumptions and taking stiff soils to have shear wave velocities above 800 m/s (site A for NTC18), we

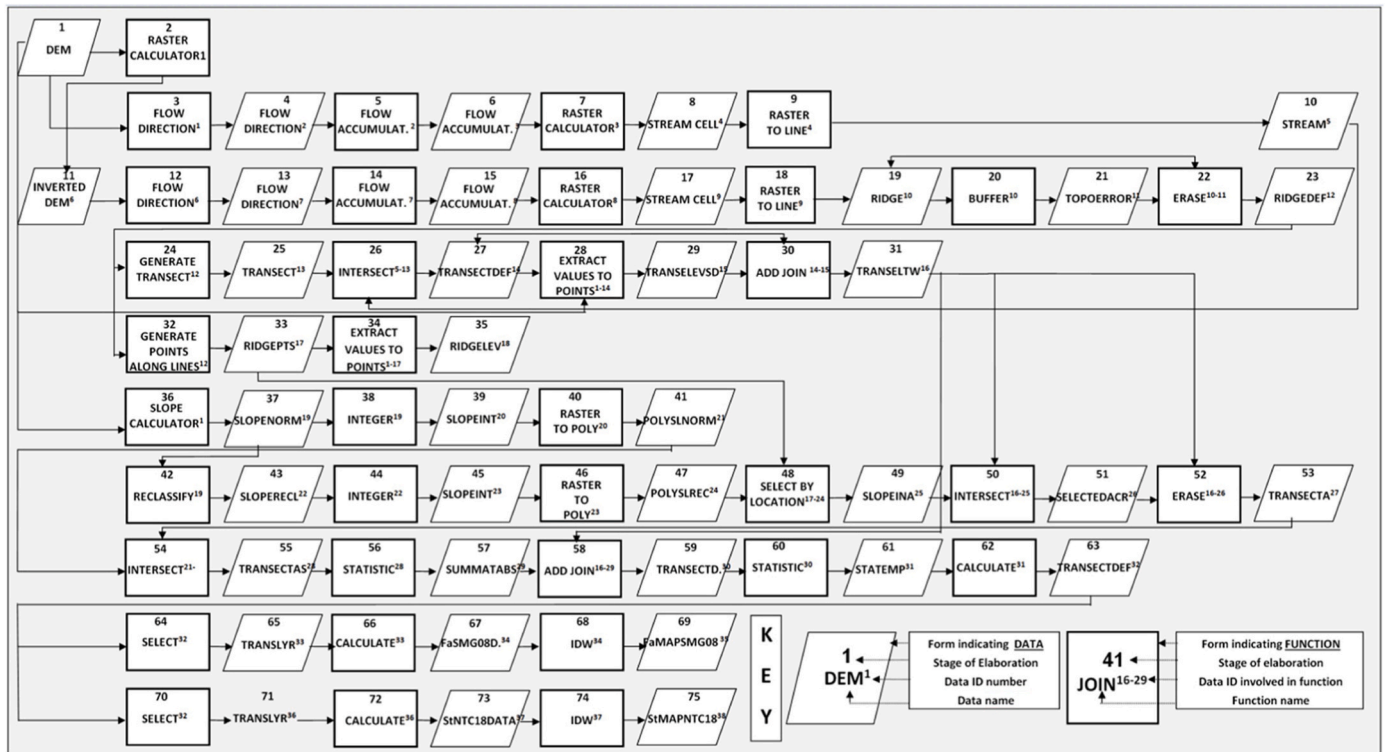


**Fig. 2.** Workflow of the numerical procedure for the automatic identification of areas prone to topographic seismic amplification effects by the current seismic codes. Additional details and excerpts of the Python code are provided in Supplementary Materials.

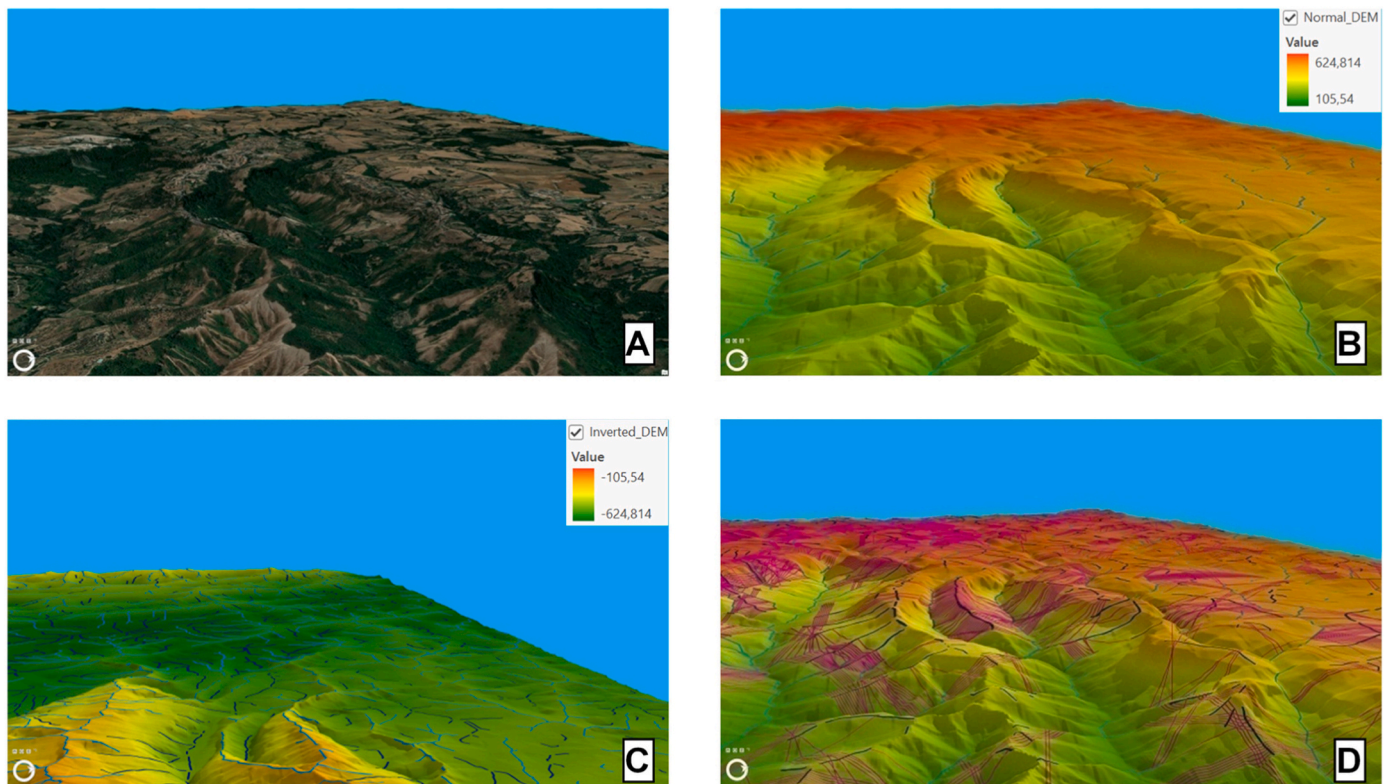


**Fig. 3.** Examples of morphometric analysis. Panel A: perspective view of a general sample area. Panel B: DEM processing results to define the flow network using the ESRI™ Spatial Analyst and Hydrology Toolset. Panel C: “Inverted DEM” processing results to define ridgelines ([43]). Panel D: results of processing to define profiles orthogonal to ridgelines. Insets of panels B and C indicate colour codes for elevation above sea level.

obtain a maximum dimension of  $L$  ( $L_{\max}$ ) of the order of 1000 m and in the case of a perfectly symmetric hill  $L \leq I + 2 \cdot W$ . Since  $I \ll L$  (we assume  $I < L_{\max}/3$ ),  $I < 300$  m and  $W_{\max} \approx 300$  m. Parametric numerical study of these landforms [21] suggests that  $h_{\max} \approx \lambda/5$ , so  $h_{\max}$  ranges from 160 to 200 m. Considering the maximum value of  $I$ ,  $W$  and  $\beta$  in order to define the bounding value of  $W_{\max}$ , we obtain  $h_{\max} \approx 160$  m and, since  $W_{\max} = h_{\max}/\tan(\beta)$ ,  $W_{\max} \approx 600$  m. So assuming  $L \approx \lambda$ , this analysis is restricted to stiff outcropping soils, and disregarding vibration periods below 0.1, the smallest geomorphologic feature to consider ( $L_{\min}$ ) measures 80 m. In summary, for automatic data processing, the assumed constraints for the spatial analysis, are listed in Table 1. It is also assumed that the lowest altitude points along the profiles, coinciding with the local valley bottom, are not affected by amplification phenomena.

### 3. Morphometric analysis of topographic conditions

#### 3.1. Previous approaches

NTC18 has been applied to small-scale land classification [22–25] using the high-resolution Digital Elevation Model (DEM) and spatial and morphometric analysis available on GIS platforms. Identification of ridges was based on 30m x 30m DEM, focusing on morphometric analysis in circular buffer areas around seismic station sites [22]. Along the same lines, a classification of all of Italy [25] has been made and applied to NW India [26]. These approaches are mainly based on extensive use of the Topographic Position Index (TPI) [27] implemented in the Land Facet Analysis toolbox (Ref. [28,29]) in ESRI ArcGis™ [19]. TPI is considered a parameter sensitive to the scale of analysis [30] requiring expert-based selection of analysis window size and differential elevation (maximum-minus minimum value of elevation) in this window. TPI-based landscape classification analysis [25–29] is therefore a very time-efficient approach, as it provides preliminary information about landforms and distribution in the regional landscape. However, it

depends heavily on the scale of analysis. For analytical application, as in SMG08 and NTC18, it may not be suitable for identifying all landforms susceptible to seismic amplification, particularly for estimating the ratios of the amplitude at the top of the relief to that at its base. Due to the need for generalization (i.e. cartographic generalization [31] and scale-dependent analysis), the TPI-based approach provides low-resolution identification of landforms in landscapes with rugged and complex geomorphologic settings, such as those of mountain ranges in Italy (i.e. Alps, Apennines and their valleys and internal basins). Furthermore, any approach that introduces meaningful generalization methods prevents detailed morphometric analysis. Clear, unambiguous, comprehensive criteria are therefore necessary to overcome limitations due to method of analysis and use of TPI if automated procedures are to be used to assess site geomorphologic effects for extensive DEM-based assessments (e.g. Refs. [23,25,29]). For this purpose, other authors (Ref. [23]) have elaborated a procedure based on 20 m x 20 m DEM, identifying ridges by means of hydrological analysis tools (Flow Direction and Flow Accumulation available in Spatial Analyst and the Hydrology Toolset of ESRI™ GIS Platform) that considers other morphometric data (slope curvature, focal statistics, and general processing of raster data derived from DEM processing) as constraints. The method used by Ref. [23] to apply NTC18 is based on land classification in which flat areas beyond a certain size (so-called “large” flat areas) are not of interest for the study. The identification of such areas is expert-based and takes land characteristics into account (see examples from the Apennines where such areas are considered to belong to alluvial basins). Although a simplification criterion for the shapes to be analyzed is needed and the one proposed by Ref. [23] seems reasonable, there may be reliefs with morphologies matching the cases identified by NTC18 even in flat areas: the NTC18 regulations do not refer to mountainous, hilly or flat areas, but only to criteria of slope, differences in elevation and ridge width-to-base ratios. Regarding estimation of the latter ratios, Ref. [23] estimates within a buffer area having a minimum

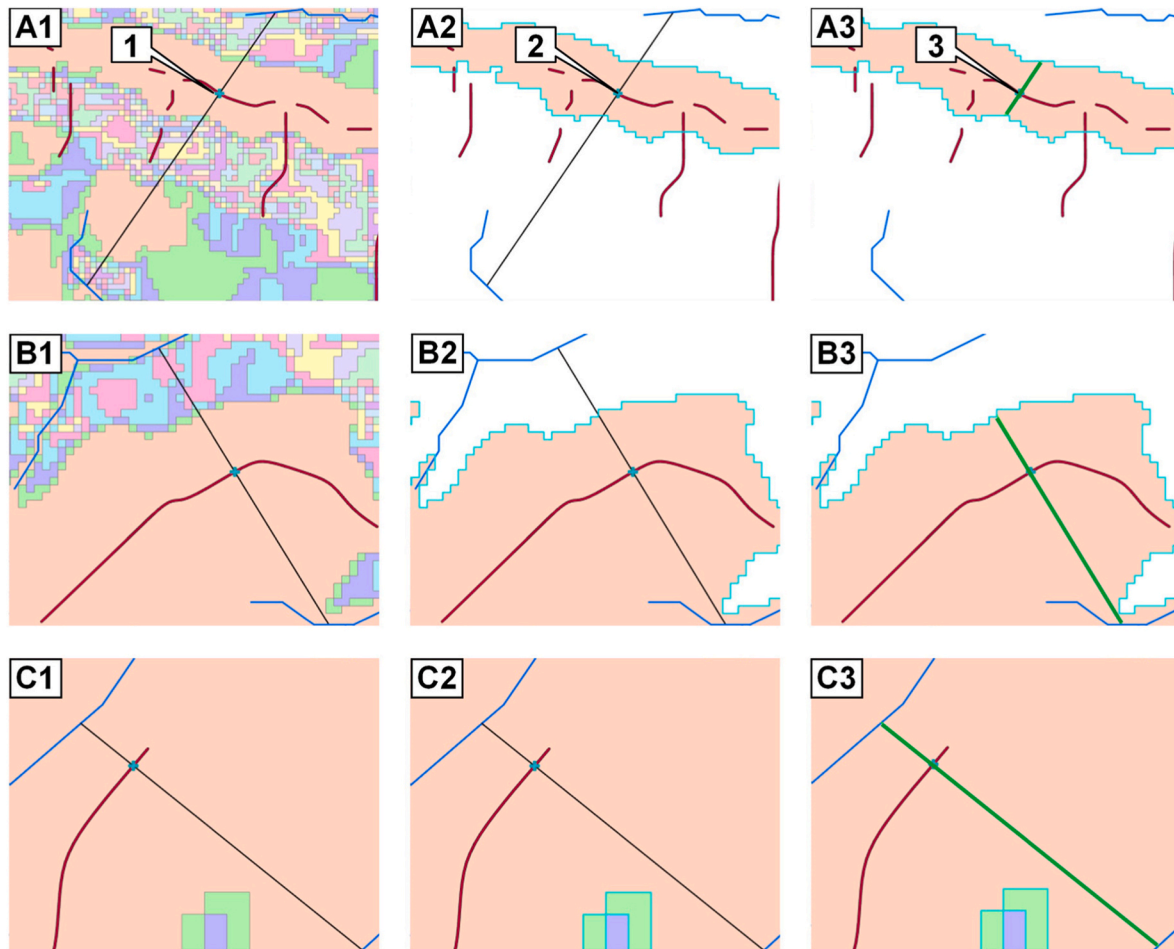


**Fig. 4.** Example of morphometric analysis to identify crests. The highest point of the ridgeline coincides with the intersection of the ridgeline and the profile (1 in panel A1). Using selection by position between the highest point and the slope polygon, we can select the slope polygon surrounding the highest elevation of the profile (2 in panel A2). Intersecting the slope polygon with the profile, we can find three intersection categories (green lines 3 in panel A3) described by SMG08/NTC18 codes: 1) isolated ridgelines (panels A3); 2) escarpments (panels B3); 3) slopes (panels C3).

width of 100 m, according to the minimum criteria established by NTC18 (slope at least  $15^\circ$  and difference in elevation at least 30 m). It is unclear how this method deals with cases where the slope extends downstream beyond the buffer area. In other terms,  $h$ ,  $H$ ,  $\alpha_1$  and  $\alpha_2$  (Fig. 1 and Table 1) are determined in this buffer area even when the slope is much longer and farther from the valley, i.e. from the base of the slope. In practice, the method proposed by Ref. [23] considers NTC18 conditions in a buffer area, while in our opinion (and according to generally accepted morphological schemes), NTC18 conditions apply to the entire slope, from the ridge top to the base of the slope.

### 3.2. Alternative ridge-detecting approach

A multiscale-multiresolution approach mitigates limitations due to scale and generalization of the results. Our data processing relies on professional GIS platforms, which provide standard analysis tools for major spatial analysis functions, both raster and vector. Here we used ESRI™ ArcGIS Pro™, and its programming language ArcPy™, but any advanced professional GIS platform could be used by adapting the code. The proposed spatial analysis methods are summarised in the flow chart of Fig. 2 and include the followings general steps (for more details about the GIS procedures and ArcPy™ codes used, see Supplementary Materials):

1. Use of DEMs for automatic extraction of the vector database for boundary lines, streams and slopes;
2. Automatic creation of regularly spaced morphological sections (profiles) orthogonal to ridges (in some references defined as crest, also);
3. Spatial analysis of profiles based on slope and length to assess the morphometric data required by SMG08 and NTC18;
4. Classification of profiles according to SMG08 and NTC18 categories and entry of classification results in a spatial database.
5. Based on the classification, calculation of  $F_a$  and  $St$  values for each profile, also entered in the database;
6. Use of stored data to map seismic hazard and topographic amplification effects, mainly for civil defence and earthquake engineering analysis. The data can be processed by users according to their needs, preferences and equipment, e.g. using spatial statistics (e.g. IDW, Kriging, line density, etc. Ref. [32–35]).

The procedure depends primarily on the availability of a DEM of appropriate resolution for the aims [36]: DEMs for Italy are widely available and we used TINITALY data provided by the CNR [37,38], available for the whole country at a spatial resolution of 10 m. This DEM was obtained from a mosaic of DEMs for single administrative regions of Italy and the data is freely available as a grid with 10 m cells (in GeoTIFF format), in the UTM WGS 84 zone 32 projection [38] that we projected to WGS 1984 UTM Zone 33 N. The DEM TINITALY was obtained mainly by processing with established techniques the elevation curves and elevation points available on topographic maps, which in turn were acquired through photogrammetric interpretation procedures. For

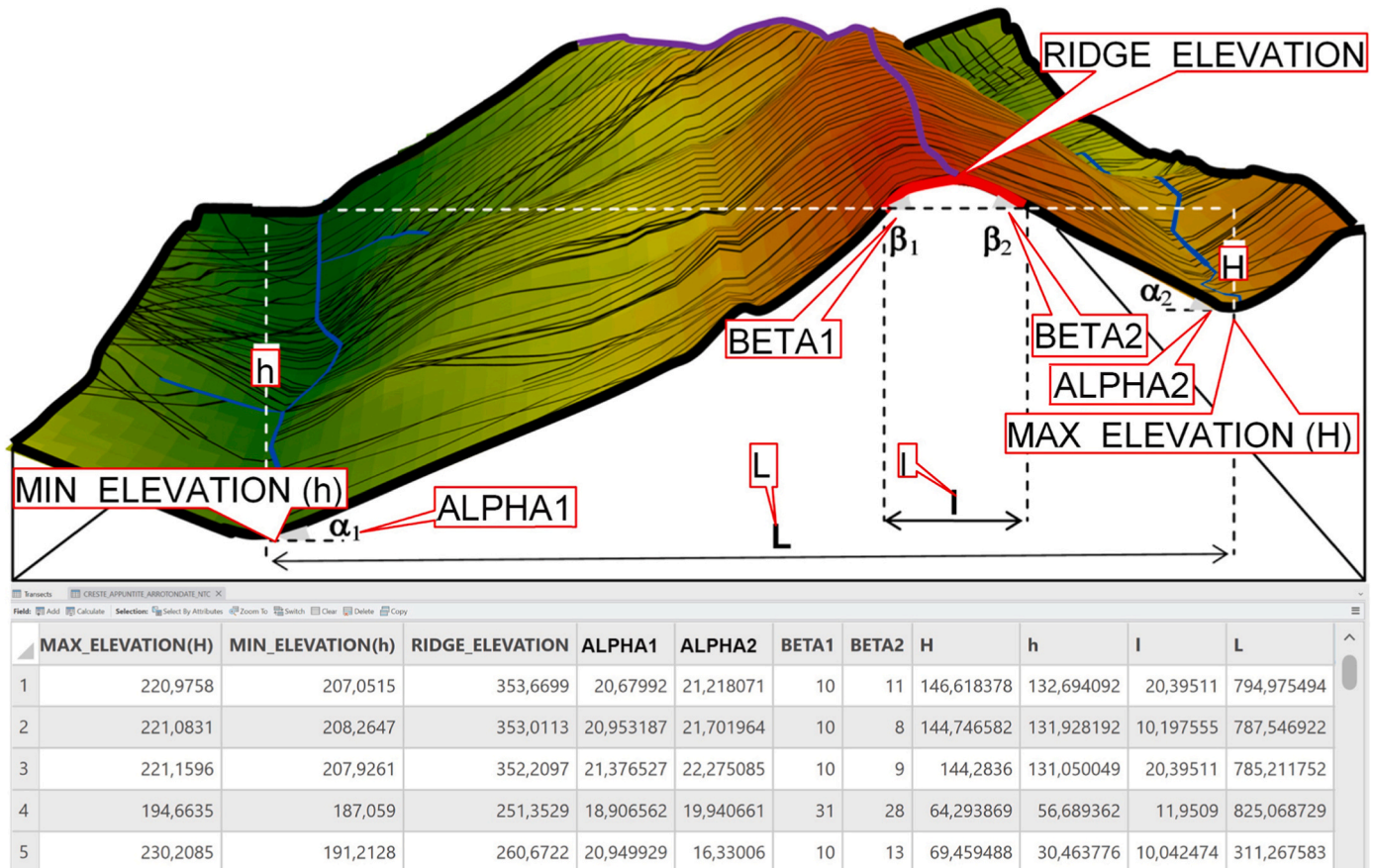


Fig. 5. Morphometric values representative of standard morphological configurations for a single profile. The meanings of the table attribute values are described in the red callout boxes in the sketch.

Table 2  
Fa values for ridges by the SMG08 code.

RidgeType	L > 350 m	250 < L < 350 m	150 < L < 250 m	L < 150
Pointed ridge	$Fa = e^{1,11H/L}$	$Fa = e^{0,93H/L}$	$Fa = e^{0,73H/L}$	$Fa = e^{0,4H/L}$
Rounded ridge	$Fa (0,1-0,5) = e^{0,47H/L}$			

Table 3  
Fa values for scarps by the SMG08 code.

Elevation class	Slope class	Fa value
10 m ≤ H ≤ 20 m	10° ≤ α ≤ 90°	1.1
20 m ≤ H ≤ 40 m	10° ≤ α ≤ 90°	1.2
H ≥ 40 m	10° < α ≤ 20°	1.1
	20° < α ≤ 40°	1.2
	40° < α ≤ 60°	1.3
	60° < α ≤ 70°	1.2
	α > 70°	1.1

regional technical cartography (CTR) at a scale of 1:10.00, which a important source of data, the technical standards for acquisition and testing stipulate a positional accuracy that does not exceed 2.5 m in planimetry and 5.00 m in elevation for areas with an average slope greater than 5% [39]. The accuracy of the DEM used in our work can be considered comparable with these accuracy values. The recent availability of very high-resolution DEMs (VHR DEMs) (e.g., airborne LIDAR surveys and 1:2000 scale mapping) makes it possible to obtain

metric-sized data that allow very detailed land analyses. Unfortunately, the availability of such data is not continuous throughout the country because these acquisitions are targeted at areas of high hydrogeological risk or intensely urbanized areas. At present, therefore, a 10 m resolution DEM such as that of TINITALY may be a good compromise in several cases: from a comparison made by Ref. [40] based on different geomorphic processes, it has been shown how it is possible to deal with these processes using a 10 m resolution DEM such as that of TINITALY, and how the availability of next-generation VHR DEMs, while it can contribute significantly to improving the analysis, does not introduce indispensable improvements over most applications, including seismic risk analysis, that make extensive use of these data [41].

As first step we run the Flow Direction and Flow Accumulation functions on DEM [42]; we set the threshold of several cells on this data by applying the Raster Calculator to define the minimum flow cells for a stream. We obtain the feature class (i.e., vector polyline) of the stream network (panels A and panel B in Fig. 3) using the Raster to Line function. Similarly, we invert the cell values using the Raster Calculator function to multiply the DEM by -1, and we obtain the ridgeline feature class by the process described for streams [43]. To remove the saddle area between closed ridges (around the peaks), we perform a buffer and topological check to identify and remove the narrow overlap area resulting from the buffer areas. The network of streams and corresponding ridgelines is now ready for further processing. On the basis of these landforms, we run the Generate Transects Along Lines function to create profiles orthogonal to the ridgelines with a user-defined spacing interval. We set the spacing between profiles at 10 m (panel D in Fig. 3), the same resolution as the DEM. The effective length of each profile is defined by the Intersection function between the generated profile and the watercourses bordering the ridgelines (Fig. 3). After creation of the

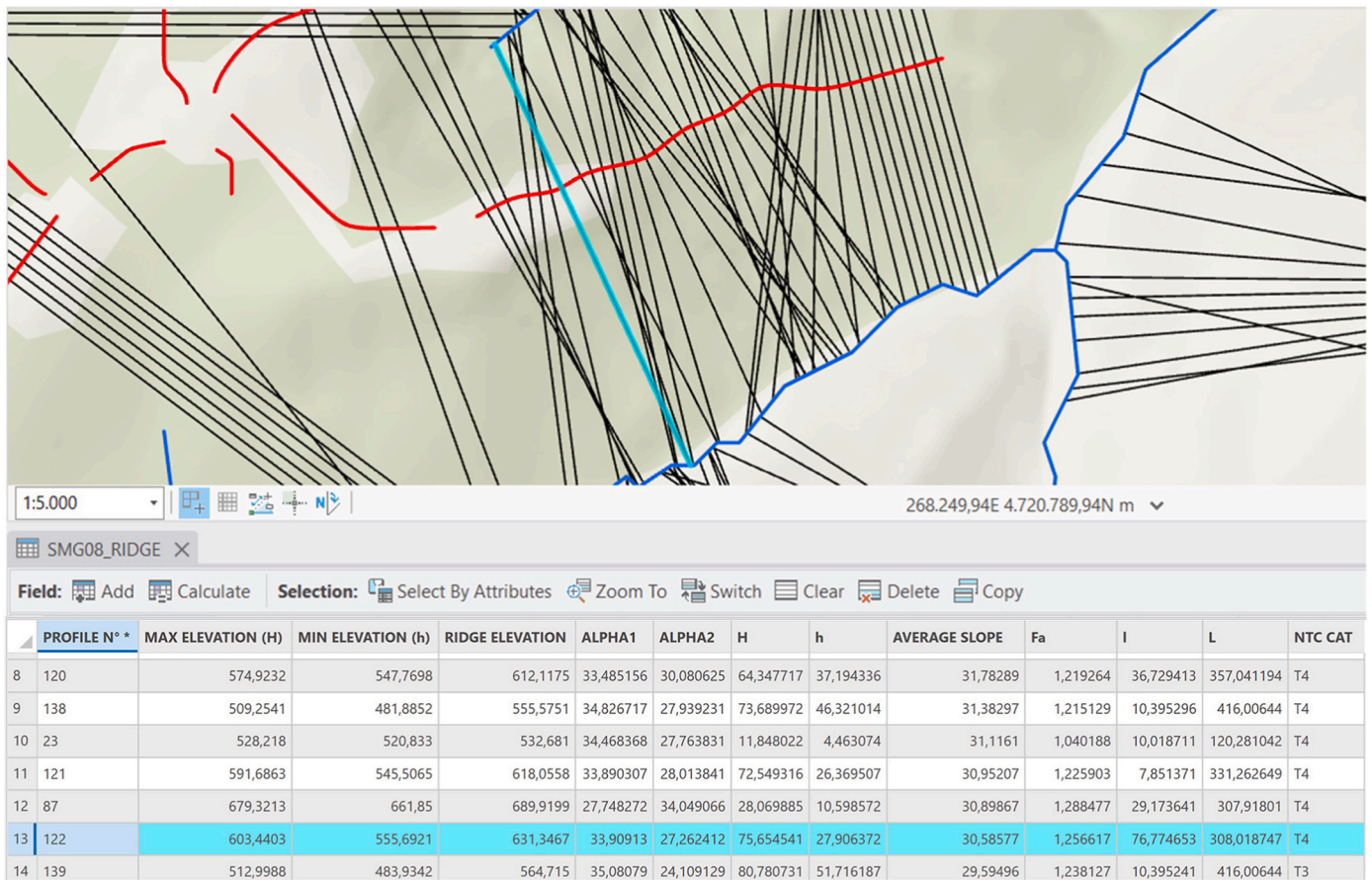


**Fig. 6.** Example of Fa (SMG08) and St (NT18) calculations. Consider the profile highlighted in cyan in the map and table (for meanings of attributes, see Fig. 3): MAX\_ELEVATION(H), MIN\_ELEVATION(h) and RIDGE\_ELEVATION values allow calculation difference of elevation from top of the hill and the bottom of the walleys. The factors  $\beta_1$ ,  $\beta_2$  and  $l$  are obtained by intersecting the profile line with slopes  $\alpha_1$  and  $\alpha_2$ .  $L$  is the length of the profile between its intersections with the watercourses. Using a SQL query on this data, the type of landform can be defined (Fig. 1) and Fa calculated (Fig. 1 and Table 1). In this case, the equation refers to appointed ridge with  $L > 350$  m ( $Fa = e^{1.11H/L}$ ) and  $Fa = 1.418047$ . For the calculation of St, a query procedure allows the selection of profiles that meet the criteria of Table 4. The red lines in the map are ridges, the black lines are profiles, and the blue lines are valley bottoms. The Fa and St values in the table are the maximum values of the ridgetops.

**Table 4**

Equations for estimating St based by NTC08 codes. Maximum expected amplification effect is assumed to depend on the steepness of the profile and is expected to occur 'near the top edge' of the plateau. The mean slope inclination is indicated as "i".

Topographic category	Topographic surface characteristics	Location of the work and intervention	ST
T1	Flat surface, isolated slopes and elevations with mean slope $i \leq 15^\circ$	-	1.0
T2	Slopes with mean inclination $i > 15^\circ$	At the top of the slope	1.2
T3	Reliefs with width at crest (I) much less than width at base (L) and average inclination $15^\circ \leq i \leq 30^\circ$	At the crest of a relief with an average slope less than or equal to $30^\circ$	1.2
T4	Reliefs with width at crest (I) much less than width at base (L) and average inclination $i > 30^\circ$	At the crest of a relief with an average slope greater than $30^\circ$	1.4

profiles, the elevations at the lowest points, i.e., stream intersections, and at hilltops along the ridgeline are obtained using the Extract Values function at points and then an Add Join function at the profile lines. At this stage of the procedure, each profile line has its own elevation i.e., the "h"s and "H"s discussed earlier. Creation of these profiles at the same

resolution as the DEM allows very detailed analysis of the morphology of the area, without loss of information (panels C and D in Fig. 3).

Another key factor in the procedure is the derivation and processing of slope data along the profile. Slope values are obtained from the DEM using the Slope Calculator function, and the resulting data is then reclassified according to SMG08 and NTC18 slope categories and converted from raster to polygon to have a slope polygon feature class more suitable for spatial analysis. The morphology resulting from intersections between the slope polygon and the profile surrounding the ridge line can be interpreted according to the SMG08 and NTC18 classifications of landforms. These codes give the morphologies different values of amplification factors Fa and St:

1. the intersection of the slope polygon and the profile defines a limited portion of the profile surrounding the ridgeline (the highest point of the profile), e.g., the isolated crest line of SMG08 and NTC018 (see panels A in Fig. 4);
2. the intersection delimits a stretch of profile that extends from the ridge to a stream on one side of the ridge, e.g., the scarp (see panels B in Fig. 4);
3. the intersection of the slope polygon and the profile completely covers the profile line from one stream intersect to the opposite stream, passing through the crest line: e.g., the hillside or slope (see panels C in Fig. 4)

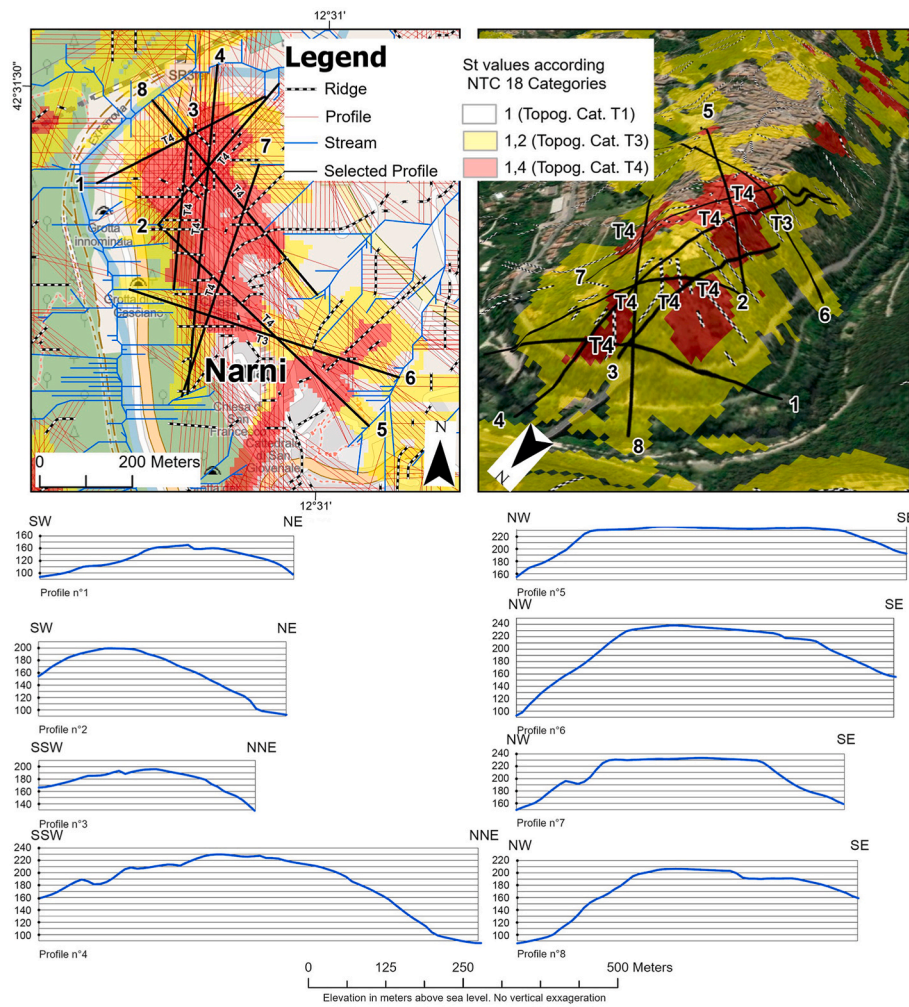


**Fig. 7.** Morphometric analysis relative to the Narni area (CentralItaly). Around this hill, in an area of 10 km2, we made 4000 topographic profiles perpendicular to the ridges of the area spaced 10 m apart, 300 of them perpendicular to the main ridge analyzed by Refs. [10,46], and represented in 2D and 3D maps above in this figure. A selection of the representative profiles (for their geographic distribution in the study area) with data on slope, length, etc. according to NTC18 code is available in this figure and data reported in Table 5.

**Table 5**

Selection of the representative profiles in the Narni area according to NTC 18. Along the ridge area of Narni, our results show the presence of topographic category T4 of NTC18 in the northern, western, and central parts, with average slopes between 30° and 35°, and the widespread presence of topographic category T3, with slopes less than 30°, in the rest of the ridge. For an explanation of symbol used in table, see Fig. 7.

Test area	Profile n°	MAX ELEV. (H)	MIN ELEV. (h)	RIDGE ELEV.	ALPHA1 (α1)	ALPHA (α2)	H	h	l	AVERAGE SLOPE	NTC CAT	L
Narni	1	709	692	738	19	27	45	29	10	23	T3	615
Narni	2	720	711	780	21	25	69	60	95	23	T3	432
Narni	3	711	681	737	15	27	56	26	20	21	T3	570
Narni	4	694	693	713	18	19	19	19	13	18	T3	198
Narni	5	703	694	753	24	21	59	50	60	22	T3	334
Narni	6	697	691	736	19	16	45	39	13	18	T3	345
Narni	7	750	721	787	17	21	66	36	14	19	T3	420
Narni	8	696	691	749	20	16	58	53	4	18	T3	402

Once the profiles have been processed, further processing based on the spatial relationships with the slope values is performed for each profile, determining the morphometric parameters (Fig. 1 and Table 1) that are finally stored in attribute tables of the spatial database (Fig. 5). On the basis of data recorded for any profile in its attribute table, we can calculate Fa and St as follows: SMG08 assesses expected site amplification by Amplification Factor (Fa), whereas NTC18 expresses St, the ratio of the average value of the response spectrum (acceleration) of ground motion impinging the relief to that expected at the surface; the average is computed by considering an interval of periods included in the range [0.5\*Ta, 1.5 Ta] where Ta is the period coinciding with the maximum of the corresponding response spectrum. Fa takes different values in relation to landform (Table 2 and Table 3); we can use this tabular data to

calculate Fa for any transect, as in the example of Fig. 5, and associate the resulting value with the profile attribute table of the spatial database (Fig. 6).

Amplification effects are also expressed in the form of the frequency-independent scalar coefficient St (NTC18, Fig. 1 and Table 1) calculated where the minimum height h of the relief is 30 m. Moreover, the maximum expected amplification effect depends on the steepness of the profile and is expected to occur ‘near the top edge’, whereas along the slopes this value is scaled linearly to value 1 at the base of each slope. We can use this tabular data (Fig. 6 and Table 4) to calculate St for any profile, as in the example of Fig. 6.

Summarizing, once the morphometric parameters (I, H, h, L and α; Fig. 6 and Table 4) have been calculated for each profile, it is possible to

**Table 6**

Morphometric characteristics of representative profiles for Assisi, Nocera Umbra and Navelli. For an explanation of symbol used in table, see Fig. 5. Alpha1, Alpha2, Average Slope in degree; Max Elev., Min Elev., H, h, l, in meters.

Test area	Profile n°	MAX ELEV. (H)	MIN ELEV. (h)	RIDGE ELEV.	ALPHA1 ( $\alpha_1$ )	ALPHA2 ( $\alpha_2$ )	H	h	l	AVERAGE SLOPE	NTC CAT.	L
Assisi	1	260	248	307	17	29	59	47	10	23	T3	478
Assisi	2	323	302	375	30	28	73	52	28	29	T3	284
Assisi	3	291	248	332	21	24	84	41	80	22	T3	405
Assisi	4	342	325	382	31	23	58	40	52	27	T3	280
Assisi	5	355	343	421	28	24	79	66	41	26	T3	439
Assisi	6	383	327	426	28	20	99	43	21	24	T3	423
Assisi	7	305	249	351	25	26	102	45	10	26	T3	380
Assisi	8	271	249	312	22	25	63	41	11	23	T3	302
Nocera	1	460	458	531	21	24	74	72	71	23	T3	450
Nocera	2	474	424	531	29	15	107	58	11	22	T3	607
Nocera	3	487	429	543	26	17	114	56	154	21	T3	603
Nocera	4	443	429	538	37	31	109	95	12	34	T4	445
Nocera	5	446	437	508	30	31	71	61	20	31	T4	406
Nocera	6	459	432	475	31	32	43	16	4	32	T4	177
Nocera	7	440	438	496	34	28	58	55	15	31	T4	277
Nocera	8	467	435	546	27	26	111	79	71	27	T3	446
Navelli	1	709	692	738	19	27	45	29	10	23	T3	615
Navelli	2	720	711	780	21	25	69	60	95	23	T3	432
Navelli	3	711	681	737	15	27	56	26	20	21	T3	570
Navelli	4	694	693	713	18	19	19	19	13	18	T3	198
Navelli	5	703	694	753	24	21	59	50	60	22	T3	334
Navelli	6	697	691	736	19	16	45	39	13	18	T3	345
Navelli	7	750	721	787	17	21	66	36	14	19	T3	420
Navelli	8	696	691	749	20	16	58	53	4	18	T3	402

associate the corresponding values of Fa and St with each profile (Fig. 6). Each profile is therefore characterized by its amplification effect coefficients according to SMG08 and NTC18 associated with a detailed spatial database of Fa and St values which can be used to make maps for hazard and risk analysis and civil protection. The data can be accessed as tables, spreadsheets or vector and raster maps suitable for data modelling, statistic and geostatistic analysis platforms.

#### 4. Case studies

We tested the proposed numerical procedure in some case studies. In particular, we compared morphological classifications provided by practitioners involved in seismic response and micronation studies with the outcomes of the proposed approach when applied to the same areas. Then, a regional scale application of the code is provided to show its potentiality in large scale studies. Detailed map and table data for SMG08 and NTC18 codes are shown as an example of output of the proposed method.

##### 4.1. NTC18 proxies

According to Ref. [25] topographic amplification has been analyzed at several sites Refs. [2,44–50]), and as a comparison with these references, we applied our methods in the municipalities of Narni, Nocera Umbra, Assisi and Navelli (Central Italy). In all these sites the presence of a slope (e.g. NTC18 Category T2) was not found or plays a negligible role. The results of our work are shown in Fig. 7: around the Narni hill, we made 4000 topographic profiles spaced each other for 10 m, 300 of them perpendicular to the main ridge analyzed by Refs. [2,49]. Our results show the presence of topographic category T4 of NTC18 in the northern and western and central parts of the ridge, with average slopes between 30° and 35°, and the widespread presence of topographic category T3, with slopes less than 30°, in the rest of the area. Our results are in good agreement with those of the cited Refs. [2,25,49], and details are available in Fig. 7 and Table 5.

The main ridge of Assisi was studied by Refs. [25,44]; in these references an amplification perpendicular to the main axis of the ridge leading to NTC18 category T3 is shown, and this result is in good agreement with our study, which predicts the same NTC18 category T3 for the entire ridge area (Fig. 7). According to Ref. [25] in this area there

is also the T4 class for the WWN edge of the ridge; therefore, we emphasize that although we do not find the NTC18 T4 category, we find there are several average slope values that are very close to the limit value of 30° (see the data for Assisi selected profiles Nos. 2, 4, 5 and 7 in Fig. 7 and Table 6).

The Nocera Umbra hillside is elongated in the NNW-SSE direction, with medium to low slope gradient in the northern slope, which increases in value toward the southern slope where the slope gradient is very steep. This morphology is well represented by the selected profiles of Nocera Umbra (Nos. 5, 6, 7 and 8 in Fig. 8 and Table 6.), and these values induce for our computations the presence of NTC18 category T3 for the northern part and NTC18 category T4 for the southern part of the ridge, in agreement with the results of Ref. [2,46–48].

The Navelli hill has a NW-SE oriented ridge and was studied by Refs. [2,25,45]. According to Ref. [25] the inclination of the slopes on the north side of the ridge (where the historical center is located) is medium-low (19°) which leads to the NTC18 category of T2. The medium-low morphological setting is also confirmed by our study (see the data of the selected profiles of Navelli n. 4, 6, 7,8 and 8 in Fig. 7 and Table 6), but since according to our results the profiles can be classified as a ridge the NTC category of T3 is present for the whole studied area. Further data about these test areas are available in Supplementary Materials.

##### 4.2. SMG08 proxies

To test the methods for the SMG08 code Cingoli area (Central Apennines, Fig. 9), where detailed Seismic Microzonation (SM) data are available. SM represents the assessment of Local Seismic Hazard by identifying and mapping areas homogeneous from the seismic point of view (Seismically Homogeneous Microzone or SHM).

For each area a representative Fa value is estimated to estimate 1D stratigraphic amplification effects. Moreover, by using the approaches proposed by Ref. [21] for slope and Refs. [15,17] for isolated reliefs and ridges, morphological amplification effects are also estimated. By following the code, these effects must be considered as relevant only in the case they are larger than the stratigraphic ones. Based on expert judgment, practitioners in charge for the seismic microzonation activities estimated the Fa values in Fig. 9 by both considering stratigraphical and topographical effects. Our analysis indicates that Fa values have

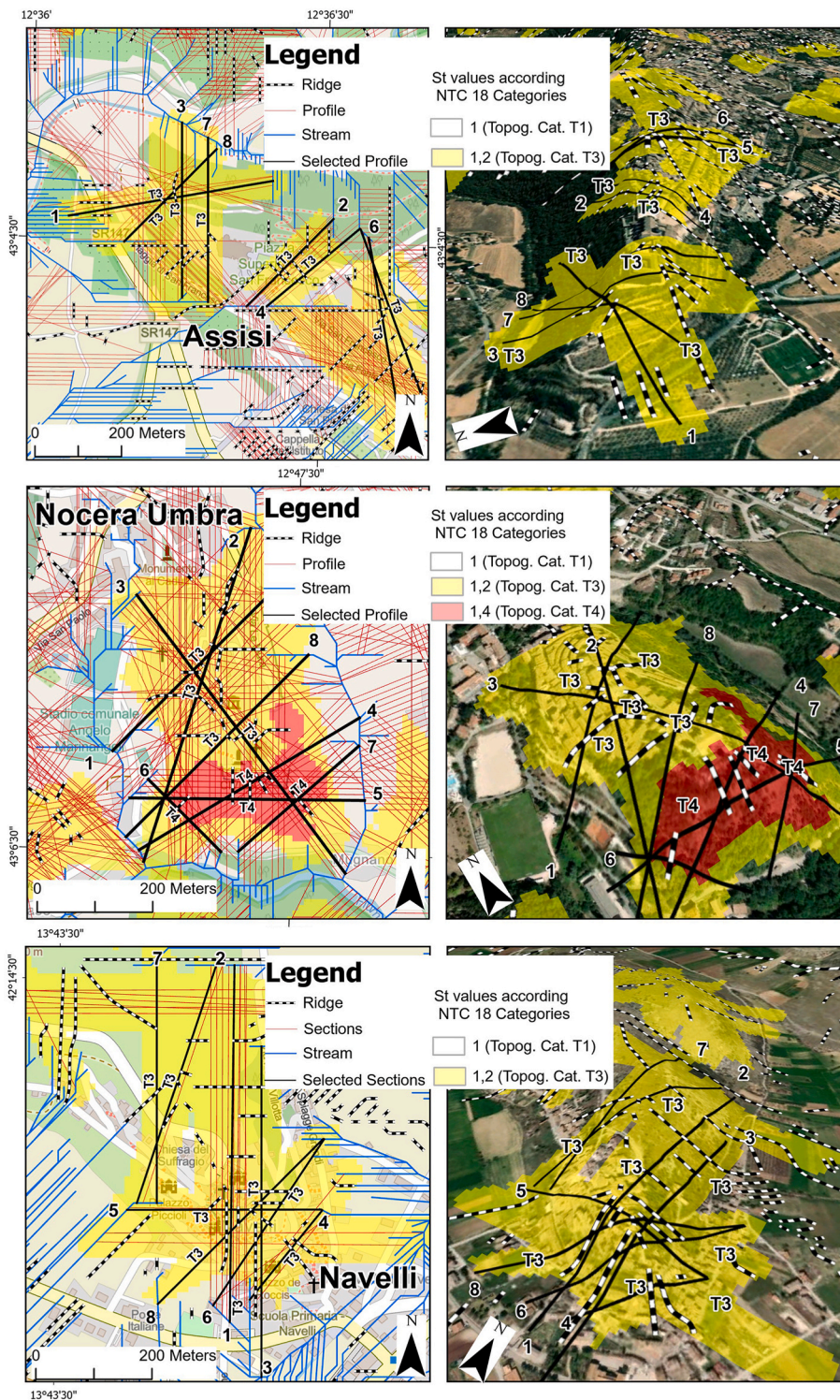


**Fig. 8.** Morphometric analysis at the sites Assisi, Nocera Umbra and Navelli (respectively in the upper, central and lower frame). In all these sites the presence of slope (e.g. NTC 18 Category T2) has not been found or is negligible. To classify the area surrounding the main ridges according to the NTC18 category, 200, 150 and 160 profiles spaced 10 m apart from each other were elaborated for the area of Assisi, Nocera Umbra and Navelli, respectively. Data for representative profiles (for their geographic distribution in the study area) for any area are provided in the 2D and 3D maps above and in [Table 1](#).

been misevaluated by the practitioner. At SW of the area, much larger Fa values have been obtained by applying the classification procedure here proposed.

#### 4.3. Application to the Marche region

This test was performed to check the feasibility of the procedure for larger areas [Fig. 10](#) The area is in the Umbro-Marchean Apennine (central Italy), a southeastern sector of the northern Apennines belt. This

orogenic system belongs to the circum-Mediterranean deformational belts created by collision of the African and European plates. After the collisional stage, the whole area underwent sedimentation of shallow water to continental deposits. Late Miocene to Quaternary tectonic uplift led to the formation of the present landscape of the region [\[51–53\]](#). Different morphostructural domains [\[6,54,56\]](#) can be recognized at regional scale:

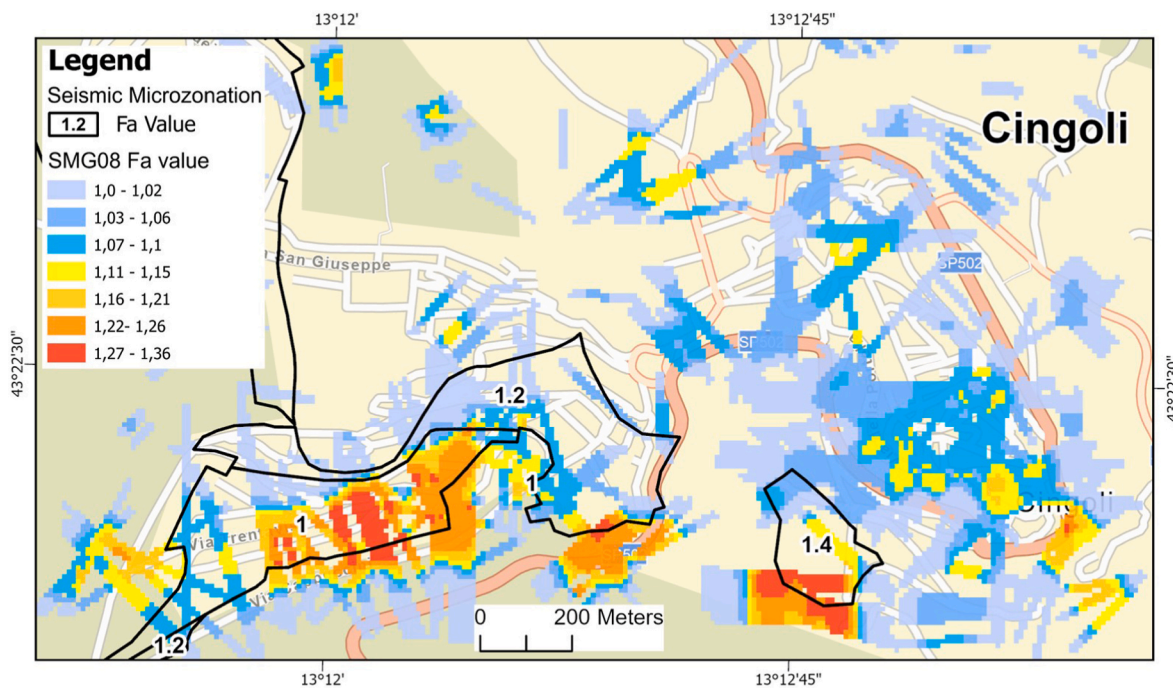


Fig. 9. Map of the Fa value for Seismic Microzonation polygons and SMG08 Fa values estimated with our methods. As stressed in the text our analysis turns out to be more detailed than the SM polygons and our Fa values are locally very different; SW of the area there are polygons with Fa = 1 according to SM, and included between 1.22 and 1.36 for our estimates. In the western part of the study area, the SM polygons have an Fa value greater than 2.0 which, according to our estimate, values are no greater than 1.36. Generally our approach gives lower Fa-values with a narrower distribution than SM polygons.

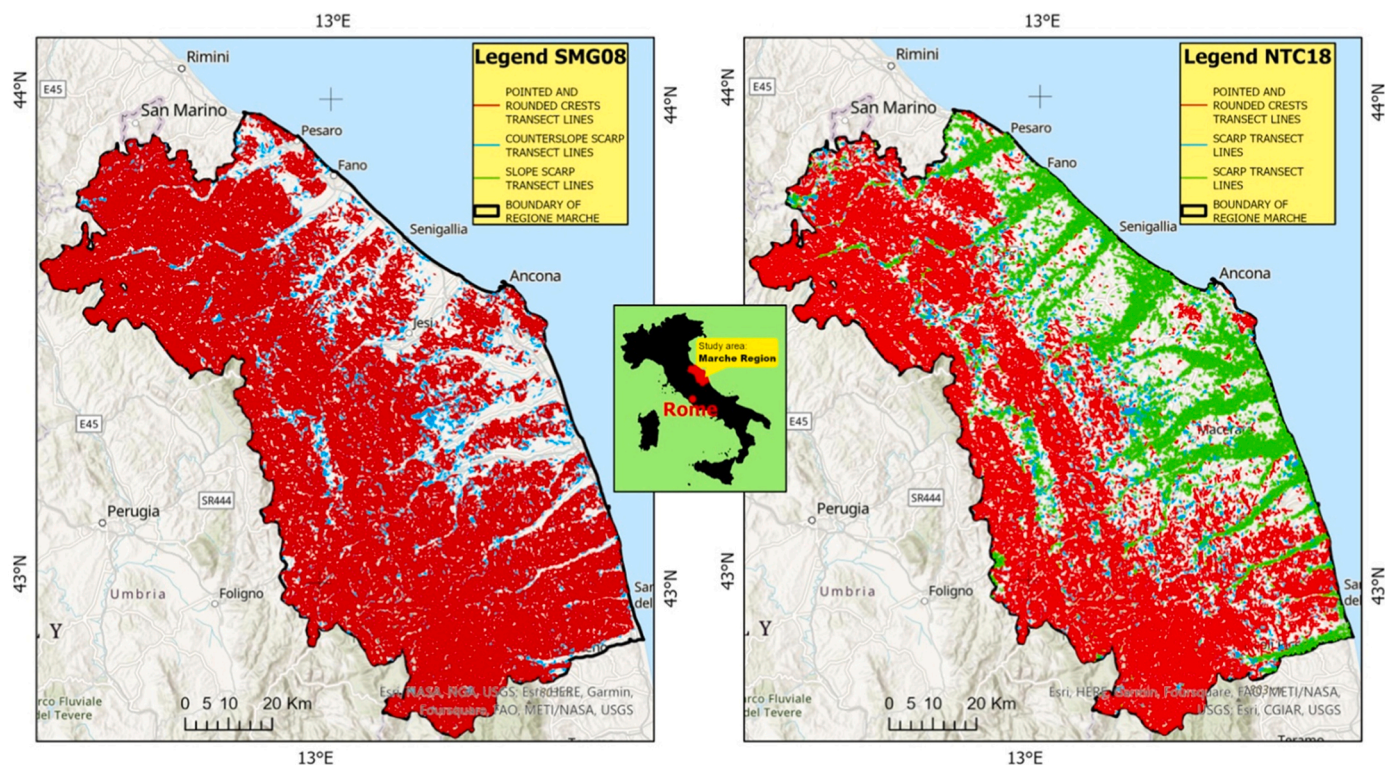


Fig. 10. The results in terms of SMG08 (left) and NTC18 (right) for the Marche region.

1. mountain ridges of mainly Triassic-Oligocene limestone of the Umbro-Marchean succession [51] with elevations exceeding 2000 m and steep to very steep slopes;
2. Foothills of Oligocene-Miocene marls and limestones [55] with elevations up to 1000 m and gentle to steep slopes;
3. terrigenous hills of Messinian sandstones and clays, with altitudes generally below 800 m;
4. Periadriatic hills of Pliocene-Lower Pleistocene marine clays and sands of the Periadriatic Basin [52] sloping gently to steeply down to the northern Adriatic shores.

**Table 7**  
Comparison of the morphometric analysis performed according to NTC18 and SMG08 codes.

Description of Morphometric Typology	Quantity
Number of ridge lines	115.586
Total length of ridge lines (Km)	23.009
Number of profile lines, 10 m spaced perpendicular to ridge lines	2.305.946
Number of profile lines suitable for NTC/SMG08 analysis	1.932.090
Total length of profile lines (Km)	1.537.122
Number of pointed/rounded crests profile lines according NTC18 code	216526
Number of scarp profile lines line according NTC18	15575
Number of slope profile lines NTC18	117728
Number of pointed/rounded crests profile lines according SMG08 code	371815
Number of "slope" scarp profile lines according SMG08	4
Number of "counterslope" scarp profile lines according SMG08	51359

The landscape is therefore rugged with sharp reliefs delimited by basins and depressions containing continental deposits. Active and seismogenic faults are also present. Applying our method, the 10 m spacing interval between profiles was extended to the whole Region. The results show that the number of sharp and rounded ridges differed according to whether NTC18 or SMG08 codes were used (Fig. 10, Table 7), ridges detected by NTC18 being about 58% of those detected by SMG08. The difference is mainly due to the slope threshold of the different codes (10° for SMG08 and 15° for NTC18) and the maximum/minimum elevation threshold (h and H) (10 m for SMG08 and 30 m for NTC18). The selection of scarps also differed for the same reason (main slope  $\alpha \geq 15^\circ$  for NTC18, and  $\geq 10^\circ$  for SMG08, Fig. 10). Results in Fig. 10 clearly at what extent the different classification criteria adopted by the two codes may affect final outcomes, well beyond the respective parameterizations in terms of St or Fa factors.

This difference is made more evident in Fig. 11 where amplification coefficients have been attributed to census districts by using the map available from ISTAT [57]. To this purpose, a spatial database of these

areas with the appropriate values of Fa and St was determined by merging the values into a new raster map and using Zonal Statistics as Table Function (Arc GIS Pro™ geoprocessing tools), classified each district by the minimum and maximum values of Fa and St occurring in each area. The values for each area were then joined to the census district map so that the polygon could be classified on the basis of the magnitude of the Fa and St values. Results in Fig. 11 makes clear that, beyond the numerical differences between Fa and St values, the extension of the areas potentially interested by topographic amplification effects are dramatically different.

### 5. Conclusion

A new effective numerical methodology has been presented to identify areas where proxies provided by current seismic codes suggest to the presence of seismic amplification phenomena induced by a class of morphological features. The method is implemented by normal GIS functions using the Python programming language and the ESRI ArcPy™ library available in ArcGIS Pro™ GIS. The kernel of the proposed approach is selection of profiles perpendicular to ridges without any topographical generalization to estimate the parameters considered in the proxies provided by the Italian codes (SMG08 and NTC18). It would also be easy to adapt our method to the any other standard. For each profile, the morphometric parameters necessary for the identification of the reference profiles are provided in the form of tabular data, accessible as a spatial database. Then, the amplification effects provided in the code are quantified at each considered site; this georeferenced data repository allows any type of map to be made and processed: raster, vector, interpolated IDW and so forth, according to user needs, e.g. for civil defence or engineering purposes. Our processing allows maps with the same resolution as the source DEM to be created. The only topographic simplifications and similar trade-offs are those related to DEM resolutions, DEM acquisitions and the algorithms available in GIS platforms for deriving slope data and hydrological toolsets. Despite efforts to

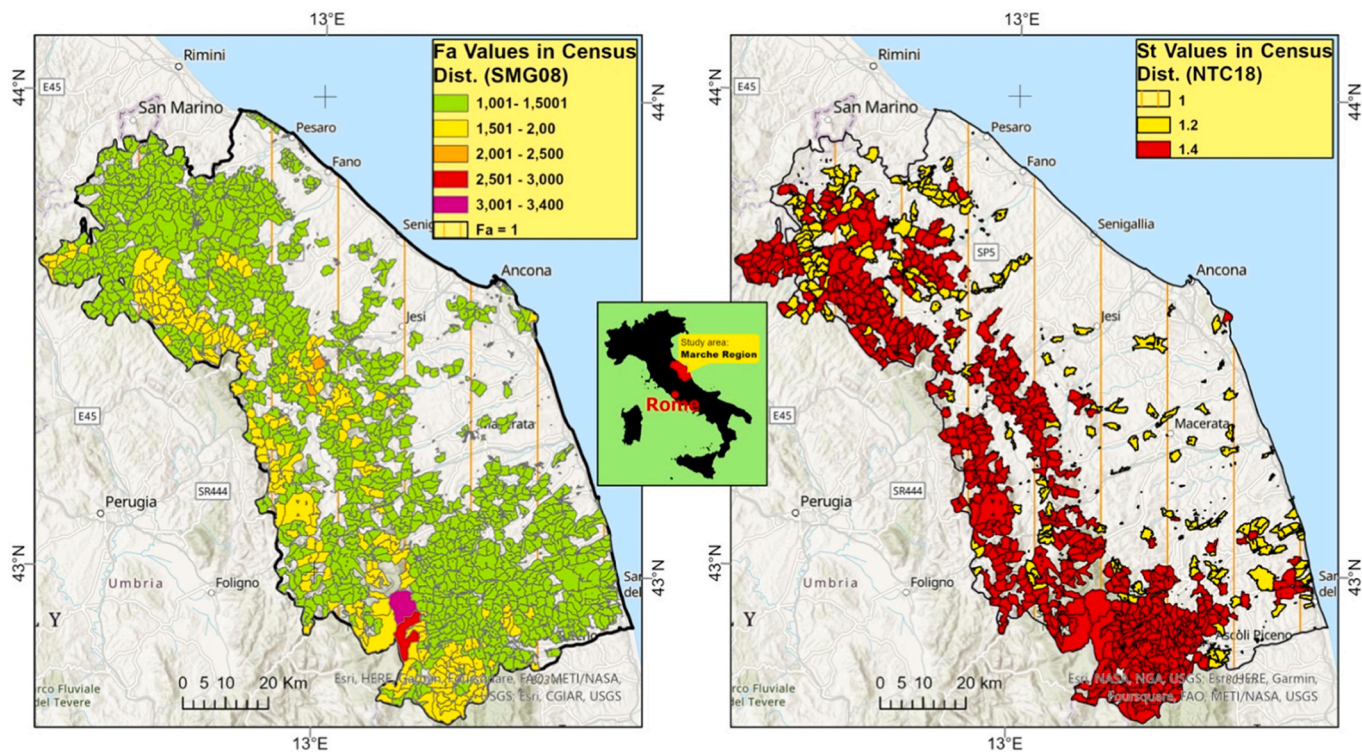


**Fig. 11.** Left: Map of maximum Fa values recorded in the census districts of the Marche region. The polygons of the census districts shown on the map are those with area having Fa values over 20% of the total. Right: Map of maximum St values recorded in the census districts of the Marche region. The polygons of the census districts shown on the map are those with area having by St values over 20% of the total.

reduce the influence of expert or empirical decisions the results, the approach relies on a number of assumptions about major parameters, needed to compensate for incompleteness of the description of the proxies proposed in the codes. These assumptions concern the vibration period of seismic waves of interest for anti-seismic design (shear waves) and the stiffness of the subsoil, which is assumed to coincide with seismic bedrock (shear wave velocity  $>800$  m/s). Different assumptions can also be considered instead of the above ones. In any case, additional constraints with respect to those of the codes are necessary to apply any of the relevant proxy. The aim of the work is to overcome these difficulties by identifying an automatic analysis workflow that allows the identification of sites possibly subject to seismic topographical amplification effects, which unlike those currently proposed in the bibliography allows to eliminate ambiguity on the choices of the analysis and excessive generalizations of geometric data and morphological maps. The proposed methods are based on numerical procedures based on spatial analysis and finally provide detailed maps and data where such effects are possible (and in some cases documented, as demonstrated for the test area), producing a detailed mapping of the dangerous zone areas in the light of current codes on seismic risk. Finally we can evaluate that on the basis of the method described above and the discussions relating to the key test area, our approach allows to overcome most of the difficulties that emerged by analytically and automatically identifying the sites possibly subject to seismic topographic amplification effects, which unlike of the approaches currently proposed in the bibliography allows to eliminate ambiguity on the analysis choices and excessive generalizations of the morphological, geometric and cartographic data, producing detailed data and maps available in spatial databases. No attempt was made here to evaluate the effectiveness of the proxies; this has been done elsewhere (e.g. Ref. [15]). For example, it results that by applying the formulas relating to SMG08 (see Table 2.), the general rule that usually the seismic amplification factor of a slope increases as the slope angle increases, is not always respected; but to the extent that these considerations are valid we cannot enter into this question because it is far beyond the scope of our work, which considers the prescriptions of the code as they are. Anyway, the univocal application of the code is a basic pre-requisite for any validation procedure based on numerical or empirical studies. Moreover, the outcomes of the present analysis may be useful to identify other combinations of the geometrical parameters of ridges and crests common in the present landscape but not considered in the codes. These could be the topic of new numerical studies to develop more effective proxies. The use of computerized techniques based on spatial analysis, geomorphometry, and other GIS tools is a common basis for much of the cited work dealing with aspects of topographic effects. In summary, the strengths of our proposal lie in the fact that, by overcoming some of the limitations used in other approaches, mainly inherent in the limitations of using the Topographic Position Index, it provides an accurate dataset related to each morphological profile of ridges and escarpments according to the codes of NTC18 and SMG08. From this point of view, it is emphasized that the values of  $St$  and  $Fa$ , inherent in NTC18 and SMG08, respectively, while both dealing with the analysis of topographic effects, have profoundly different meanings. The possibility of having both of these values for the same area means that, comparing the value of  $Fa$  with the topographic coefficient ( $ST$ ), one can adopt the more onerous of the two or carry out local deepening as provided, for example, by Level 3 Seismic Microzonation. The limitations of our approach are reduced if not absent, our methods being dependent on the accuracy of the DEM. In this sense, however, we emphasize that, regardless of the proposed methods of analysis, there are obvious critical issues in the use of the NTC18 and SMG08 codes arising from all the uncertainties in the application of the regulations that we have tried to mitigate with the premises described in section 2 of this paper. Further progress could be made by modelling crucial areas where our method detects maximum values of  $Fa$  and  $St$ , coupling these areas with geological data, particularly stratigraphy and engineering geology, and with measured geophysical data (i.e.

measured  $V$  and other geophysical properties of soils and subsoils). The proposed method and geological and geophysical data finally make it possible to test the reliability of SMG08 and NTC18 codes.

### Author statement

**Pier Lorenzo Fantozzi:** being a GIS expert with a long experience in managing spatial databases in Earth Sciences and for seismic risk mitigation, this author's contribution is related to data analysis and information requirements of NTC18 and SMG08 codes (current official codes for mitigation events). In addition, this author defined the many steps of spatial analysis for automatic target morphology detection and wrote the Python™ and ArcPy™ code. Even the testing and construction phases of most of the figures, maps and tables are the responsibility of this author.

**Pierluigi Pierucini:** he is a senior geomorphologist and in this work he evaluated the correspondences of the results of the spatial analysis with the identification of the real morphology prone of inducing topographical effects of seismic amplification.

**Enrico Paolucci** he is a seismologist and his task in this article is to evaluate the results with other areas where seismic amplification by topographic effects has been described. He is also in charge of comparing our results with the place where the SMG08 codes have been applied by experienced practitioners and since then evaluate the scientific input and finalize of the proposed methods.

**Dario Albarello:** he is full professor of seismology and boasts a long experience in seismic mitigation activity, with collaboration with Italian Civil Protection and other public bodies; in this paper his contribution evaluated the results and how they could improve the availability of the data, their accuracy and correspondence with the needs of the stakeholders.

### Declaration of competing interest

The authors declare that they have no known competing financial interests or personal relationships that could have appeared to influence the work reported in this paper.

### Data availability

Data will be made available on request.

### Acknowledgements

The study has been developed in the frame of the SERENA Project. Granted by Ministry of University and Research, Projects of Relevant National Interest - year 2020 (PRIN). Code: 2020MMCPER. Public Body: University of Siena, Italy. Coordinator Prof. Albarello Dario. Title: Mapping seismic site effects at regional and national scale.

### Appendix A. Supplementary data

Supplementary data to this article can be found online at <https://doi.org/10.1016/j.soildyn.2023.108212>.

### References

- [1] Bard PY, Riepl-Thomas J. Wave propagation in complex geological structures and their effects on strong ground motion. In: Kausel E, Manolis G, editors. *Wave motion in earthquake engineering*. UK: WIT Press; 1999.
- [2] Massa M, Lovati S, D'Alema E, Ferretti G, Bakavoli M. An experimental approach for estimating seismic amplification effects at the top of a ridge, and the implication for ground-motion predictions: the case of Narni, Central Italy. *Bull Seismol Soc Am* 2010;100(6):286–301. <https://doi.org/10.1785/0120090382>.
- [3] Panizza M. Geomorphology and seismic risk. *Earth Sci Rev* 1991;31:11–20. [https://doi.org/10.1016/0012-8252\(91\)90040-M](https://doi.org/10.1016/0012-8252(91)90040-M).

- [4] WGS (Working Group on Seismic Microzoning - Gruppo di lavoro MS. Indirizzi e criteri per la microzonazione sismica. Conferenza delle Regioni e delle Province autonome 2008. Rome: Dipartimento della Protezione Civile; 2008 [in Italian]).
- [5] NTC. Ministero delle Infrastrutture e dei Trasporti. Aggiornamento delle Norme Tecniche per le Costruzioni. Part 3.2.2: categorie di sottosuolo e condizioni topografiche, 42. Gazzetta Ufficiale n; 2018. del 20 febbraio 2018 (in Italian).
- [6] Pieruccini P, Paolucci E, Fantozzi PL, Naldini D, Albarello D. Developing effective subsoil reference model for seismic microzonation studies: Central Italy case studies. *Nat Hazards* 2021;24. <https://doi.org/10.21203/rs.3.rs-804952/v1>.
- [7] Thorn Colin E. An introduction to theoretical geomorphology. Unwin Hyman; 1988. p. 247. <https://doi.org/10.1007/978-94-010-9441-2>.
- [8] Scheidegger Adrian E. Limitations of the system approach in geomorphology. *Geomorphology* 1992;5:213–7. [https://doi.org/10.1016/0169-555X\(92\)90004-8](https://doi.org/10.1016/0169-555X(92)90004-8).
- [9] Rhoads L, Thorn Colin E. *Observation in geomorphology*. John Wiley & Sons Ltd; 1996.
- [10] Pike RJ, Evans IS, Hengl T. Geomorphometry: a brief guide. *Dev Soil Sci* 2009;33: 3–30. [https://doi.org/10.1016/S0166-2481\(08\)00001-9](https://doi.org/10.1016/S0166-2481(08)00001-9).
- [11] Carrara A. Multivariate models for landslide hazard evaluation. A "black box" approach', Workshop on Natural Disasters in European Mediterranean Countries, Perugia, Italy. 1988. p. 205–24.
- [12] Carrara A, Cardinali M, Detti R, Guzzetti F, Pasqui V, Reichenbach P. GIS techniques and statistical models in evaluating landslide hazard. *Int J Rock Mech Min Sci Geomech Abstr* 1991;29:A102. <https://doi.org/10.1002/esp.3290160505>.
- [13] Van Westen CJ, Van Duren I, Kruse HMG, Terlien MTJ. GISSIZ: training package for geographic information systems in slope instability zonation. ITC-Publication Number; 1993. p. 15 [ITC, Enschede].
- [14] Rovelli A. Review of recent data on surface topography effects. Network of European Research Infrastructures for Earthquake Risk Assessment and Mitigation; 2011. p. 101.
- [15] Paolucci R. Amplification of earthquake ground motion by steep topographic irregularities. *Earthq Eng Struct Dynam* 2002;31:1831–53. <https://doi.org/10.1002/eqe.192>.
- [16] Gatmiri B, Kamalian M. Combination of boundary element and finite element methods for evaluation of dynamic response of saturated porous media. In: *Proceedings of the 5th European conference on "numerical methods in geotechnical engineering"*; 2002. Paris.
- [17] Pagliaroli A, Lanzo G, D'Elia B, Costanzo A, Silvestri F. Topographic amplification factors associated to cliff morphology: numerical results from two case studies in Southern Italy and comparison with EC8 recommendations. In: *XIV European Conference on Soil Mechanics and Geotechnical Engineering, Workshop on geotechnical aspect of EC8*; 2007.
- [18] Nguyen KV, Gatmiri B. Evaluation of seismic ground motion induced by topographic irregularity. *Soil Dynam Earthq Eng* 2007;27(2):183–8. <https://doi.org/10.1016/j.soildyn.2006.06.005>.
- [19] ESRI. ArcGIS PRO : release 3.03. Redlands, CA: Environmental Systems Research Institute; 2023.
- [20] Van Rossum G, Drake FL. Python 3 reference manual. Scotts Valley, CA: Create Space; 2009.
- [21] Ashford SA, Sitar N. Analysis of topographic amplification of inclined shear waves in a steep coastal bluff. *Bull Seismol Soc Am* 1997;87:692–700. <https://doi.org/10.1785/BSSA007030692>.
- [22] Di Capua G, Lanzo G, Pessina V, Peppoloni S, Scasserra G. The recording stations of the Italian strong motion network: geological information and site classification. *Bull Earthq Eng* 2011;9(6):1779–96. <https://doi.org/10.1007/s10518-011-9326-7>.
- [23] Pessina V, Fiorini E. A GIS procedure for fast topographic characterization of seismic recording stations. *Soil Dynam Earthq Eng* 2014;63:248–58. <https://doi.org/10.1016/j.soildyn.2014.04.002>.
- [24] Scandella L, Davi M, Paolucci R, Pessina V. Numerical simulation and GIS mapping of seismic amplification due to topographic effects. In: *Proceedings of 31st European seismological commission (ESC)*. Greece: Crete; 2008.
- [25] Mascandola C, Luzi L, Felicetta C, Pacor F. A GIS procedure for the topographic classification of Italy, according to the seismic code provisions. *Soil Dynam Earthq Eng* 2021;148:106848. <https://doi.org/10.1016/j.soildyn.2021.106848>.
- [26] Agrawal N, Dixit J. Topographic classification of North-Eastern Region of India using geospatial technique and following seismic code provisions. *Environ Earth Sci* 2022;81:436. <https://doi.org/10.1007/s12665-022-10556-w>.
- [27] Weiss A. Topographic position and landform analysis. San Diego, CA: Poster presentation, ESRI Users Conference; 2001.
- [28] Jenness J, Brost B, Beier P. Land facet corridor designer. USDA forest service rocky mountain research station; 2013.
- [29] Tuba Z, Uttam P, Yuichi SH, Takashi O. Knick zone Extraction Tool (KET) - a new ArcGIS toolset for automatic extraction of knick zones from a DEM based on multi-scale stream gradients. *Open Geosci* 2017;9(1):73–88. <https://doi.org/10.1515/geo-2017-0006>.
- [30] Grohmann C, Riccomini C. Comparison of roving-window and search-window techniques for characterizing landscape morphometry. *Comput Geosci* 2009;35: 2164–5. <https://doi.org/10.1016/j.cageo.2008.12.014>.
- [31] Cebrzykow P. Elaboration of topographic bases for statistical maps, their contents and importance. *Pol Cartogr Rev* 2017;49(3):97–106. <https://doi.org/10.1515/pcr-2017-0008>.
- [32] Philip GM, Watson DF. A precise method for determining contoured surfaces. *Australian Petrol Exploration Assoc J* 1982;22:205–12. <https://doi.org/10.1071/AJ81016>.
- [33] Watson DF, Philip GM. A refinement of inverse distance weighted interpolation. *Geo Process* 1985;2:315–32.
- [34] Burrough PA. Principles of geographical information systems for land resources assessment. New York: Oxford University Press; 1986. <https://doi.org/10.1080/10106048609354060>.
- [35] Oliver MA. Kriging: a method of interpolation for geographical information systems. *Int J Geogr Inf Syst* 1990;4:313–32. <https://doi.org/10.1080/02693799008941549>.
- [36] Florinsky IV. Digital terrain analysis in soil science and geology. 2nd revised edition. Amsterdam: Elsevier Academic Press; 2016. p. 486. <https://doi.org/10.1016/B978-0-12-804632-6.00001-8>.
- [37] Tarquini S, Vinci S, Favalli M, Doumaz F, Fornaciari A, Nannipieri L. Release of a 10-m-resolution DEM for the Italian territory: comparison with global-coverage DEMs and anaglyph-mode exploration via the web. *Comput Geosci* 2012;38(1): 168–70. <https://doi.org/10.1016/j.cageo.2011.04.018>.
- [38] Tarquini S, Isola I, Favalli M, Battistini A, Dotta G. TINITALY, a digital elevation model of Italy with a 10 meters cell size (Version 1.1). Istituto Nazionale di Geofisica e Vulcanologia (INGV); 2023.
- [39] Regione Toscana, Giunta Regionale Direzione Generale Governo Del Territorio, Sistema Informativo Territoriale e Ambientale. *Prescrizioni tecniche per la cartografia fotogrammetrica numerica in scala 1:2.000 e 1:10.000 livello 4.5*, Firenze, maggio 2014. 2015. revisione 1 – maggio.
- [40] Tarquini S, Nannipieri L. The 10m-resolution TINITALY DEM as a trans-disciplinary basis for the analysis of the Italian territory: current trends and new perspectives. *Geomorphology* 2017;281:108–15. <https://doi.org/10.1016/j.geomorph.2016.12.022>.
- [41] Stucchi M, Meletti C, Montaldo V, Crowley H, Calvi GM, Boschi E. Seismic hazard assessment (2003–2009) for the Italian building code. *Bull Seismol Soc Am* 2011; 101(4):1885–911. <https://doi.org/10.1785/0120100130>.
- [42] Arc hydro tools. Tutorial. 2011., Version 2.0.
- [43] ESRI Technical Article Details. How to: identify ridgelines from a DEM. 2016. Article ID..
- [44] Cauzzi C, Fäh D, Pessina V, Faccioli E, Smerzini C. Topographic amplification from recorded earthquake data and numerical simulations. In: *15th world conference on earthquake engineering*; 2012. <http://hdl.handle.net/2122/8582>.
- [45] Gallipoli MR, Bianca M, Mucciarelli M, Parolai S, Picozzi M. Topographic versus stratigraphic amplification: mismatch between code provisions and observations during the L'Aquila (Italy, 2009) sequence. *Bull Earthq Eng* 2013;11(5):1325–36. <https://doi.org/10.1007/s10518-013-9446-3>.
- [46] Caserta A, Bellucci F, Cultrera G, Donati S, Marra F, Mele G, Palombo B, Rovelli A. Study of site effects in the area of Nocera Umbra (Central Italy) during the 1997 Umbria-Marche seismic sequence. *J Seismol* 2000;4:555–65. <https://doi.org/10.1023/A:1026510300469>.
- [47] Donati S, Marra F, Rovelli A. Damage and ground shaking in the town of Nocera Umbra during Umbria-Marche, central Italy, earthquakes: the special effect of a fault zone. *Bull Seismol Soc Am* 2001;91:511–9. <https://doi.org/10.1785/0120000114>.
- [48] Pischiutta M, Cultrera G, Caserta A, Luzi L, Rovelli A. Topographic effects on the hill of Nocera Umbra, central Italy. *Geophys J Int* 2010;182(2):977–87. <https://doi.org/10.1111/j.1365-246X.2010.04654.x>.
- [49] Lovati S, Bakavoli MKH, Massa M, Ferretti G, Pacor F, Paolucci R, Haghshenas E, Kamalian M. Estimation of topographical effects at Narni ridge (Central Italy): comparisons between experimental results and numerical modelling. *Bull Earthq Eng* 2011;9(6):1987–2005. <https://doi.org/10.1007/s10518-011-9315-x>.
- [50] Pischiutta M, Cianfarra P, Salvini F, Cara F, Vannoli P. A systematic analysis of directional site effects at stations of the Italian seismic network to test the role of local topography. *Geophys J Int* 2018;214(1):635–50. <https://doi.org/10.1093/gji/ggy133>.
- [51] Calamita F, Coltorti M, Pieruccini P, Pizzi A. Evoluzione strutturale e morfogenesi plio-quadernaria dell'Appennino umbro-marchigiano tra il pedappennino umbro e la costa adriatica. *Boll Soc Geol It* 1999;118:125–39 [in Italian].
- [52] Coltorti M, Pieruccini P. A late Lower Pliocene planation surface across the Italian Peninsula: a key tool in neotectonic studies. *J Geodyn* 1999;29:323–8. [https://doi.org/10.1016/S0264-3707\(99\)00049-6](https://doi.org/10.1016/S0264-3707(99)00049-6).
- [53] Bally AW, Burbi L, Coope JC, Ghelardoni R. Balanced sections and seismic reflection profiles across the Central Apennines. *Mem Soc Geol Ital* 1986;35: 257–310.
- [54] Amanti M, Chiessi V, Muraro C, Puzilli LM, Roma M, Catalano S, Romagnoli G, Tortorici G, Cavuoto G, Albarello D, Fantozzi PL, Paolucci E, Pieruccini P, Caprari P, Mirabella F, Della Seta M, Esposito C, Di Curzio D, Francescone M, Pizzi A, Macerola L, Nocentini M, Tallini M. Geological and geotechnical models definition for 3rd level seismic microzonation studies in Central Italy. *Bull Earthq* 2020;18:5441–73. <https://doi.org/10.1007/s10518-020-00843-x>.
- [55] Centamore E, Deiana G, Micarelli A, Potetti M. Il trias-paleogene delle Marche. In: Centamore E, Deiana G, editors. *La geologia delle Marche*. Studi Geol Camerti; 1986. p. 9–27 [in Italian].
- [56] Bigi S, Cantalamessa G, Centamore E, Didaskalou P, Micarelli A, Nisio S, Pennesi T, Potetti M. The periadriatic basin (Marche-Abruzzi sector, Central Italy) during the Plio-Pleistocene. *Giorn Geol* 1997;59:245–59.
- [57] ISTAT. Descrizione dei dati geografici dei confini delle unità amministrative a fini statistici. Versione 19/03/2020.